

Non-Hermitian band theory of directional amplification

Wen-Tan Xue,¹ Ming-Rui Li,¹ Yu-Min Hu,¹ Fei Song,¹ and Zhong Wang^{1,*}

¹*Institute for Advanced Study, Tsinghua University, Beijing, 100084, China*

The phenomenon of amplifying forward-propagating signals while blocking back-propagating ones, known as the directional amplification, is important for a wide range of applications. As open systems that exchange energy with the environment, directional amplifiers exhibit intrinsically non-Hermitian physics. General formulas for the gain and directionality, though highly desirable, have been lacking. In this work, we find these formulas in a compact and user-friendly form. This solution implies deep connections between the directional amplification and non-Hermitian topological band theory. In particular, our formulas are based on the concept of generalized Brillouin zone, which was initially introduced as a key ingredient in understanding the non-Hermitian topology. These formulas could provide a widely applicable criterion for designing directional amplifiers, and point to new potential applications based on non-Hermitian band theory.

Amplification and nonreciprocal transmission of signal are essential to a wide range of devices. Amplification compensates for the ubiquitous loss[1], while nonreciprocity enables the isolation of signal source from noises[2–8]. Traditional nonreciprocal devices such as isolators and circulators are bulky, and require magnetic field that is often adverse to device integration. Magnetic-free schemes have been proposed based on spatiotemporal modulations[9–11], nonlinearity[12], and Josephson effect[5–7]. Recently, an efficient and general method, known as reservoir engineering[13, 14], has attracted growing attentions. In this approach, nonreciprocity stems from the dissipative interactions induced by the engineered environment. This scheme has been successfully realized in optomechanical and other hybrid systems[15–19].

Irrespective of the device details, directional amplifiers are generally characterized by non-Hermitian physics, which is natural because amplifiers are open systems that exchange energy with the environment. Particularly, the time evolution of modes are generated by a non-Hermitian matrix that can be viewed as an effective non-Hermitian Hamiltonian[13–26], from which one can obtain the scattering matrix that tells the gain and directionality[13, 14, 20]. For few-mode amplifiers, the scattering matrix can be readily found by brute force. The more powerful many-mode amplifiers, however, are more complex to characterize. The simplest many-mode amplifiers, which take the shape of a one-dimensional chain of short-range-coupled modes, have the advantage of unlimited gain-bandwidth product without fine tuning[23, 24]. However, general formulas of the gain and directionality, which would provide a guiding principle for designing directional amplifiers, are lacking so far.

These key formulas are obtained in this work. Our formulas are inspired by the recently proposed non-Bloch band theory of non-Hermitian systems[27–29]. Intriguingly, some of the basic concepts of the familiar Bloch band theory have to be revised to characterize non-Hermitian bands. In particular, the standard Brillouin

zone (BZ) is replaced by the generalized Brillouin zone (GBZ)[27–37]. Although GBZ was introduced from a rather different motivation (namely non-Hermitian topology), we find that it offers surprisingly simple yet general formulas for directional amplifiers[Eq.(12-15)].

Non-Hermitian bands of amplifiers.—For concreteness, we consider a 1D lattice of coupled bosonic modes, which can be realized in various realistic systems, such as optomechanical cavities[15, 38] and photonic lattices[20, 39]. The bosonic modes are denoted by a_0, a_1, \dots, a_L , where L is the chain length. For simplicity, let all modes have the same bare frequency ω_0 , and each mode is coupled to its neighbors with strengths t_1 and t_2 [Fig. 1(a)]. Each site receives a coherent drive with amplitude $\epsilon_i(t)$, which can represent an incoming signal to be amplified. The Hamiltonian reads

$$H_0 = \sum_i [(t_1 a_i^\dagger a_{i+1} + t_2 a_i^\dagger a_{i+2} + \text{H.c.}) + \omega_0 a_i^\dagger a_i + \epsilon_i a_i^\dagger + \epsilon_i^* a_i]. \quad (1)$$

As the system is open, we consider the density matrix ρ , whose time evolution follows the quantum master equation

$$\dot{\rho}(t) = -i[H_0, \rho] + \sum_\mu \left(L_\mu \rho L_\mu^\dagger - \frac{1}{2} \{L_\mu^\dagger L_\mu, \rho\} \right), \quad (2)$$

where L_μ 's are the dissipators describing the effects of environment. While the physics is general, we take the following set of dissipators for concreteness: $\{L_\mu\} = \{L_i^g, L_i^l\}$, including the single-particle gain $L_i^g = \sqrt{\gamma} a_i^\dagger$ and loss $L_i^l = \sqrt{\gamma}(a_i - i a_{i+2})$. Feasible implementations of such dissipators have been discussed in details[13, 20].

The most measurable quantity is the field coherences $\phi_i(t) = \langle a_i(t) \rangle = \text{Tr}[a_i \rho(t)]$. It follows from Eq. (2) that they evolve under an effective non-Hermitian Hamiltonian $H[40]$:

$$\dot{\phi}_i = -i \sum_j H_{ij} \phi_j - i \epsilon_i. \quad (3)$$

For our specific model in Fig.1(a), the expression of H is[40]

$$H = \begin{pmatrix} \omega_0 + i\kappa & t_1 & t_2 - \frac{\gamma}{2} & 0 & \cdots \\ t_1 & \omega_0 + i\kappa & t_1 & t_2 - \frac{\gamma}{2} & \cdots \\ t_2 + \frac{\gamma}{2} & t_1 & \omega_0 + i\kappa & t_1 & \cdots \\ 0 & t_2 + \frac{\gamma}{2} & t_1 & \omega_0 + i\kappa & \cdots \\ \cdots & \cdots & \cdots & \cdots & \cdots \end{pmatrix}, \quad (4)$$

where $\kappa = \frac{\gamma'}{2} - \gamma$ is introduced to simplify notations. This H is shown pictorially in Fig. 1(b). The corresponding Bloch Hamiltonian reads

$$h(k) = (t_2 + \frac{\gamma}{2})e^{-2ik} + t_1e^{-ik} + \omega_0 + i\kappa + t_1e^{ik} + (t_2 - \frac{\gamma}{2})e^{2ik}. \quad (5)$$

Let us introduce the vector notation $\vec{\epsilon} = (\epsilon_0, \dots, \epsilon_L)$, and similarly for $\vec{\phi}$. For an external drive $\vec{\epsilon}$ with a fixed frequency, $\vec{\epsilon}(t) = \vec{\epsilon}(\omega) \exp(-i\omega t)$, the resultant field is $\vec{\phi}(t) = \vec{\phi}(\omega) \exp(-i\omega t)$ whose amplitude is

$$\vec{\phi}(\omega) = G(\omega)\vec{\epsilon}(\omega); \quad G(\omega) = \frac{1}{\omega - H}. \quad (6)$$

To simplify notations, we shall measure the frequency with respect to ω_0 , namely, rename $\omega - \omega_0$ as ω . As such, negative ω will denote frequencies lower than ω_0 .

The Green's function matrix G determines the amplification. For a signal entering the j site, with the only nonzero component of $\vec{\epsilon}$ being ϵ_j , the induced field at i site is $\phi_i = G_{ij}\epsilon_j$. Directional amplification occurs when $G_{ij} > 1$ while $G_{ji} \ll 1$ for a pair (i, j) , meaning that a signal is amplified from j to i site, while the opposite propagation from i to j is blocked. We are especially interested in G_{L0} and G_{0L} , which in general have the large- L behavior

$$|G_{L0}| \sim \alpha_{\rightarrow}^L, \quad |G_{0L}| \sim \alpha_{\leftarrow}^L, \quad (7)$$

or equivalently, $\log(\alpha_{\rightarrow}) = \frac{d(\log |G_{L0}|)}{dL}$, $\log(\alpha_{\leftarrow}) = \frac{d(\log |G_{0L}|)}{dL}$. Directional amplification from left to right is realized when $\alpha_{\rightarrow} > 1$, $\alpha_{\leftarrow} < 1$, while from right to left realized when $\alpha_{\rightarrow} < 1$, $\alpha_{\leftarrow} > 1$. Note that α_{\rightarrow} or $\alpha_{\leftarrow} > 1$ is possible because H is non-Hermitian. An example of $\alpha_{\leftarrow} > 1$ is shown in Fig.1(c). Notably, such 1D amplifiers do not suffer from the standard limitation of gain-bandwidth product[23, 24], because large gain is possible for large L , while the bandwidth is independent of L . They achieve such an advantage without any fine tuning.

Note that in other formulations of amplification such as the input-output formalism[1], the scattering matrix can be slightly different from G . Nevertheless, the difference is negligible because it does not grow with L [14, 24], therefore focusing on G is sufficient here.

The amplitude gain (square root of the power gain) G_{L0}, G_{0L} and the gain density $\alpha_{\rightarrow}, \alpha_{\leftarrow}$ are the key quantities of directional amplifiers. The key question is: What are their general formulas?

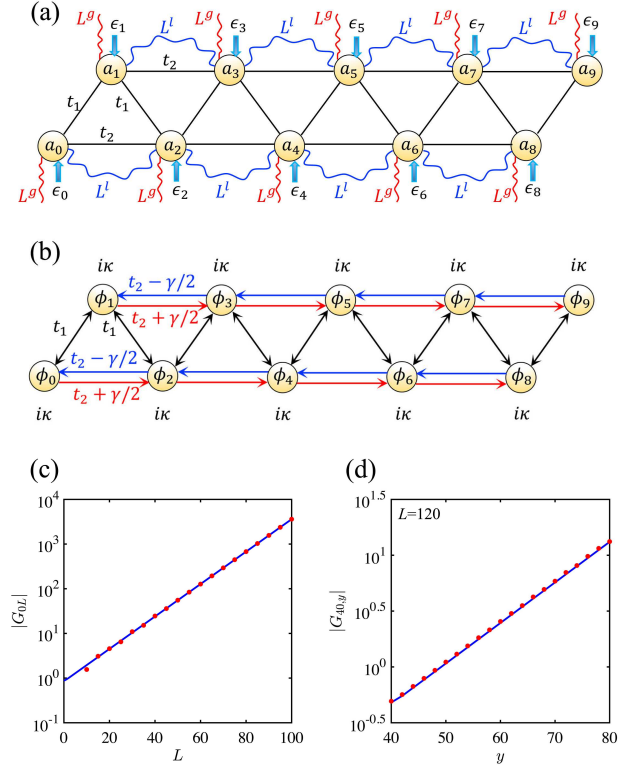


FIG. 1. (a) A chain of bosonic modes coupled by hopping $t_{1,2}$. Gain and loss are denoted by $L^{g,l}$ and the external signals by ϵ_i . We take open-boundary condition (OBC). $L = 9$. (b) The hopping Hamiltonian H for the coherence ϕ_i . (c) $|G_{0L}|$. Blue line represents Eq.(13) with $|K| = 1.817$. (d) $|G_{40,y}|$ for $L = 120$. Blue line represents Eq.(11). For (c)(d), parameters are $t_1 = 2$, $t_2 = 0.3$, $\gamma = 0.3$, $\kappa = -0.1$, and $\omega = -2.5$.

The GBZ formulas of amplifier.—A plausible starting point is the spectral representation[41] $(\omega - H)^{-1} = \sum_n (\omega - E_n)^{-1} |\psi_{nR}\rangle \langle \psi_{nL}|$, where E_n and $|\psi_{nR(L)}\rangle$ are the eigenvalues and normalized right (left) eigenvectors of H , namely, $H|\psi_{nR}\rangle = E_n|\psi_{nR}\rangle$, $\langle \psi_{nL}|H = \langle \psi_{nL}|E_n$. However, it is difficult to see from it the behavior in Eq.(7). It is tempting to switch to the momentum space or BZ, and a plausible formula is

$$G_{L0} = \int_0^{2\pi} \frac{dk}{2\pi} \frac{e^{ikL}}{\omega - h(k)}. \quad (8)$$

With the notation $\beta = e^{ik}$, BZ is the unit circle and the integral becomes $|\beta| = 1$:

$$G_{L0} = \int_{|\beta|=1} \frac{d\beta}{2\pi i \beta} \frac{\beta^L}{\omega - h(\beta)}. \quad (9)$$

One of its immediate difficulties is apparent after using the residue theorem, which leads to $G_{L0} \sim |\beta_S|^L$, β_S being the largest-modulus root of $\omega - h(\beta) = 0$ inside the unit circle. This would always imply $\alpha_{\rightarrow} = |\beta_S| < 1$ and forbids any directional amplification. In fact, Eq. (9) is generally valid only in Hermitian cases, as will be clear below.

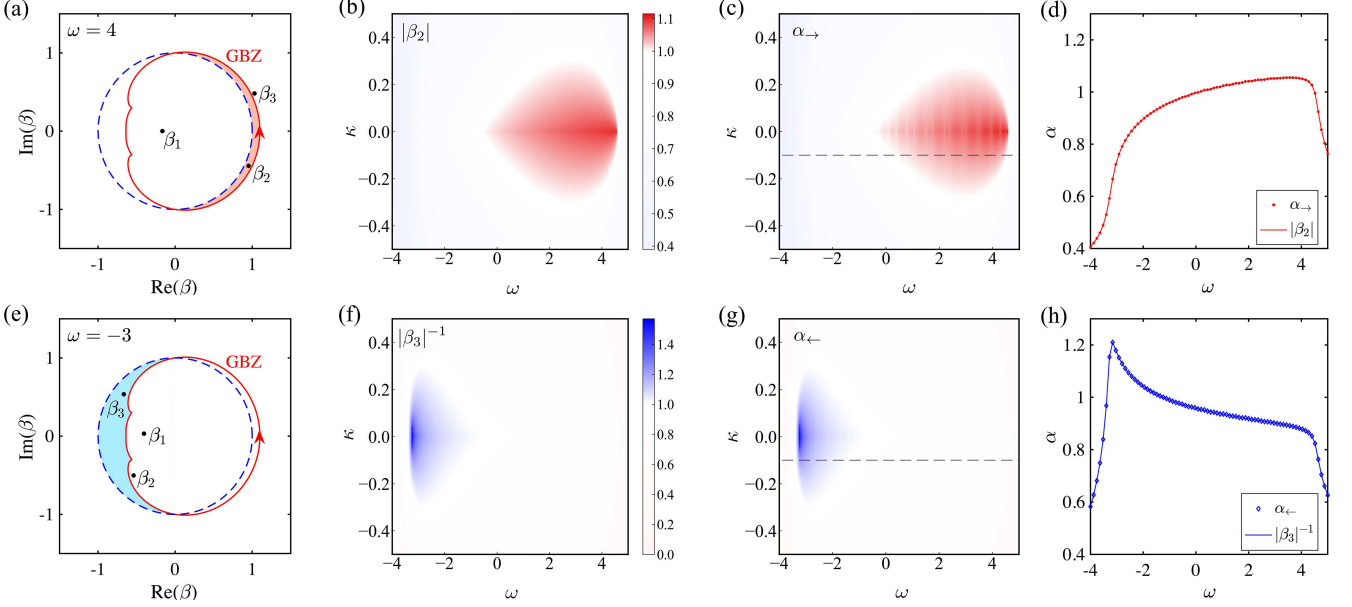


FIG. 2. (a) GBZ (red solid loop) and BZ (blue dashed circle). $\beta_{1,2,3}$ are roots of $h(\beta) = \omega$ for $\kappa = -0.1$ and $\omega = 4$ (β_4 is outside this region). (b) $|\beta_2|$ as a function of κ, ω . (c) α_{\rightarrow} from Eq.(7). (d) α_{\rightarrow} and $|\beta_2|$ along the cut $\kappa = -0.1$ [dashed line in (c)]. (e) The same as (a) except that $\omega = -3$. (f) $|\beta_3|^{-1}$. (g) α_{\leftarrow} . (h) α_{\leftarrow} and $|\beta_3|^{-1}$ along the cut $\kappa = -0.1$. Parameter values are $t_1 = 2$, $t_2 = 0.3$, $\gamma = 0.3$.

The problem with Eq. (9) is the assumption of the validity of Bloch band theory. In fact, a unique non-Hermitian phenomenon is that, for a broad class of non-Hermitian Hamiltonian, all the eigenstates are localized at the boundaries, which is known as the non-Hermitian skin effect. In other words, extended Bloch waves are replaced by boundary-localized eigenstates. Their precise description relies on the non-Bloch band theory based on GBZ. Crucially, $h(\beta)$ with β varying in the BZ and GBZ yields the continuous energy spectra for periodic-boundary condition (PBC) and open-boundary condition (OBC), respectively, and these two are generally different. In Hermitian cases, GBZ is the same as BZ, being consistent with the fact that PBC and OBC continuous spectra are the same. We summarize the needed GBZ equation as follows[27, 28]. Let M be the hopping range of H ($M = 2$ in our case), then $h(\beta) = \sum_{j=-M}^M h_j \beta^j$ with certain coefficients h_j . Now $h(\beta) = E$ is a $2M$ -th order equation with roots $\beta_1(E), \beta_2(E), \dots, \beta_{2M}(E)$, which are ordered as $|\beta_1| \leq |\beta_2| \leq \dots \leq |\beta_{2M}|$. The GBZ equation reads[27, 28]

$$|\beta_M(E)| = |\beta_{M+1}(E)|, \quad (10)$$

which is essentially a single-variable equation because β_M, β_{M+1}, E are related by $h(\beta_M) = h(\beta_{M+1}) = E$. The β_M and β_{M+1} solutions form a closed loop in the complex plane, dubbed the GBZ. It has been applied to establish the non-Bloch bulk-boundary correspondence[27, 28, 42–45].

Having GBZ in mind, one may be tempted to guess

that the largest (smallest) $|\beta|$ in GBZ determines rightward (leftward) amplification, as the corresponding eigenstate has the steepest rightward (leftward) exponential growth and seems to have dominant contributions. This conjecture is ruled out by its lacking ω dependence; in contrast, α_{\rightarrow} and α_{\leftarrow} depend on ω . The conjecture is not entirely incorrect; it turns out to be the upper bound of α_{\rightarrow} and α_{\leftarrow} .

We propose the following general formula for G_{xy} :

$$G_{xy} = \int_{\text{GBZ}} \frac{d\beta}{2\pi i \beta} \frac{\beta^{x-y}}{\omega - h(\beta)}, \quad (11)$$

which is numerically confirmed [Fig.1(d)]. A derivation is provided in Supplemental Material. The formula is precise for x, y not too close to the two ends. At the ends, because of the boundary effect, a numerical factor K of order unity has to be included:

$$G_{L0} = K \int_{\text{GBZ}} \frac{d\beta}{2\pi i \beta} \frac{\beta^L}{\omega - h(\beta)}, \quad (12)$$

$$G_{0L} = K \int_{\text{GBZ}} \frac{d\beta}{2\pi i \beta} \frac{\beta^{-L}}{\omega - h(\beta)}. \quad (13)$$

The vital fact that GBZ is a closed loop now enables application of the residue theorem. Ordering the roots of $h(\beta) = \omega$ as $|\beta_1| \leq |\beta_2| \leq \dots \leq |\beta_{2M}|$, one can prove that β_1, \dots, β_M are enclosed by the GBZ, while $\beta_{M+1}, \dots, \beta_{2M}$ are not. To see this, suppose that we vary ω in the complex plane (though ω is real-valued for physical applications). As long as ω stays away from the OBC energy spectrum E_{OBC} , the roots β_i 's cannot touch

the GBZ because GBZ generates E_{OBC} . Therefore, the number of roots enclosed by GBZ is independent of ω . To determine this number, we consider the $|\omega| \rightarrow \infty$ limit, in which either the β^M or β^{-M} term dominates $h(\beta)$ and there are M roots with $|\beta| \sim |\omega|^{1/M} \rightarrow \infty$, and also M roots with $|\beta| \sim |\omega|^{-1/M} \rightarrow 0$. Therefore, there are M roots $\beta_{1,2,\dots,M}$ inside the GBZ (For a more rigorous proof, see Refs.[46, 47]). Now Eq.(12) and Eq.(13) can be simplified by the residue theorem. For Eq.(13), the integral can be transformed to that of $\beta' = 1/\beta$, which facilitates using the residue theorem. For large L , the results read

$$G_{L0} \sim (\beta_M)^L, \quad G_{0L} \sim (\beta_{M+1})^{-L}, \quad (14)$$

in other words,

$$\alpha_{\rightarrow} = |\beta_M|, \quad \alpha_{\leftarrow} = |\beta_{M+1}|^{-1}. \quad (15)$$

Therefore, the *middle two* roots β_M and β_{M+1} determine the gain and directionality, leading to a surprising simplification. As a corollary of our formulas, the roots inside the GBZ but outside the BZ generate rightward amplification ($|\beta_M| > 1$), while those outside the GBZ but inside the BZ generate leftward amplification ($|\beta_{M+1}|^{-1} > 1$). The two regions are colored in Fig.2(a) and (e), respectively. Eqs.(11-15) are the central results of this work. For multi-band systems, Eq.(15) remains applicable with $\beta_{j=1,\dots,2M}$ denoting the roots of $\det[\omega - h(\beta)]$ [40]. Note that the significance of taking OBC for amplification has been discussed in recent insightful papers[23, 24], and the significant role of non-Hermitian skin effect was observed in Ref.[23]. The key ingredient missing in all previous studies is the GBZ, which plays a fundamental role in our formulas.

As an application to the model in Fig.1, we show in Fig.2 a quantitative comparison of our theory with the extensive numerical results. For all the parameters investigated, the numerical α_{\rightarrow} and α_{\leftarrow} are in excellent agreement with Eq.(15) with $M = 2$. Notably, the amplifier can, in a single device, selectively amplify signal in a frequency-dependent direction. In our theory, this frequency-dependent directionality is possible when the GBZ has intersections with the BZ [Fig.2(a,e)]. This picture provides a mechanism for designing devices that efficiently integrate directional amplifiers and frequency filters or splitters. On the other hand, the simpler cases of rightward (leftward) unidirectional amplification within the entire bandwidth are realized when the GBZ is entirely outside (inside) the BZ (an example is shown in Supplemental Material).

Discussion.—The central results of this work are general formulas of gain and directionality for directional amplifications, which could provide an efficient and general guide for designing high-quality directional amplifiers. The general approach reveals a surprisingly simple and precise connection between directional amplification

and non-Hermitian topological band theory, which suggests novel applications based on the non-Hermitian band concepts. Notably, our formulas can also be viewed as a solution to one of the most natural problems in the non-Hermitian band theory, namely the linear response of non-Hermitian bands. From this perspective, the solution also raises many intriguing questions for future studies in non-Hermitian bands, such as the interaction effects that are significant in certain hybrid systems.

Acknowledgements.—We would like to thank Hongyi Wang for helpful discussions. This work is supported by NSFC under Grant No. 11674189. WTX, MRL, YMH, FS contributed equally to this work.

* wangzhongemail@gmail.com

- [1] A. A. Clerk, M. H. Devoret, S. M. Girvin, Florian Marquardt, and R. J. Schoelkopf, “Introduction to quantum noise, measurement, and amplification,” *Rev. Mod. Phys.* **82**, 1155–1208 (2010).
- [2] Dirk Jalas, Alexander Petrov, Manfred Eich, Wolfgang Freude, Shanhui Fan, Zongfu Yu, Roel Baets, Miloš Popović, Andrea Melloni, John D Joannopoulos, *et al.*, “What is-and what is not-an optical isolator,” *Nature Photonics* **7**, 579–582 (2013).
- [3] Liang Feng, Maurice Ayache, Jingqing Huang, Ye-Long Xu, Ming-Hui Lu, Yan-Feng Chen, Yeshaiah Fainman, and Axel Scherer, “Nonreciprocal light propagation in a silicon photonic circuit,” *Science* **333**, 729–733 (2011).
- [4] Christophe Caloz, Andrea Alù, Sergei Tretyakov, Dimitrios Sounas, Karim Achouri, and Zoé-Lise Deck-Léger, “Electromagnetic nonreciprocity,” *Phys. Rev. Applied* **10**, 047001 (2018).
- [5] Baleegh Abdo, Katrina Sliwa, Luigi Frunzio, and Michel Devoret, “Directional amplification with a josephson circuit,” *Phys. Rev. X* **3**, 031001 (2013).
- [6] Baleegh Abdo, Katrina Sliwa, S. Shankar, Michael Hatridge, Luigi Frunzio, Robert Schoelkopf, and Michel Devoret, “Josephson directional amplifier for quantum measurement of superconducting circuits,” *Phys. Rev. Lett.* **112**, 167701 (2014).
- [7] K. M. Sliwa, M. Hatridge, A. Narla, S. Shankar, L. Frunzio, R. J. Schoelkopf, and M. H. Devoret, “Reconfigurable josephson circulator/directional amplifier,” *Phys. Rev. X* **5**, 041020 (2015).
- [8] Romain Fleury, Dimitrios L Sounas, Caleb F Sieck, Michael R Haberman, and Andrea Alù, “Sound isolation and giant linear nonreciprocity in a compact acoustic circulator,” *Science* **343**, 516–519 (2014).
- [9] Dimitrios L Sounas and Andrea Alù, “Non-reciprocal photonics based on time modulation,” *Nature Photonics* **11**, 774–783 (2017).
- [10] Zongfu Yu and Shanhui Fan, “Complete optical isolation created by indirect interband photonic transitions,” *Nature photonics* **3**, 91 (2009).
- [11] Nicholas A Estep, Dimitrios L Sounas, Jason Soric, and Andrea Alù, “Magnetic-free non-reciprocity and isolation based on parametrically modulated coupled-resonator loops,” *Nature Physics* **10**, 923–927 (2014).
- [12] Marin Soljačić, Chiyan Luo, John D Joannopoulos,

- and Shanhui Fan, “Nonlinear photonic crystal microdevices for optical integration,” *Optics letters* **28**, 637–639 (2003).
- [13] A. Metelmann and A. A. Clerk, “Nonreciprocal photon transmission and amplification via reservoir engineering,” *Phys. Rev. X* **5**, 021025 (2015).
- [14] Leonardo Ranzani and José Aumentado, “Graph-based analysis of nonreciprocity in coupled-mode systems,” *New Journal of Physics* **17**, 023024 (2015).
- [15] Kejie Fang, Jie Luo, Anja Metelmann, Matthew H Matheny, Florian Marquardt, Aashish A Clerk, and Oskar Painter, “Generalized non-reciprocity in an optomechanical circuit via synthetic magnetism and reservoir engineering,” *Nature Physics* **13**, 465–471 (2017).
- [16] Shabir Barzanjeh, Matthias Wulf, Matilda Peruzzo, Mahmoud Kalaei, PB Dieterle, Oskar Painter, and Johannes M Fink, “Mechanical on-chip microwave circulator,” *Nature communications* **8**, 1–7 (2017).
- [17] G. A. Peterson, F. Lecocq, K. Cicak, R. W. Simmonds, J. Aumentado, and J. D. Teufel, “Demonstration of efficient nonreciprocity in a microwave optomechanical circuit,” *Phys. Rev. X* **7**, 031001 (2017).
- [18] Nathan Rafaël Bernier, Laszlo Daniel Toth, A Koottandavida, Marie Adrienne Ioannou, Daniel Malz, Andreas Nunnenkamp, AK Feofanov, and TJ Kippenberg, “Non-reciprocal reconfigurable microwave optomechanical circuit,” *Nature communications* **8**, 1–8 (2017).
- [19] H Xu, Luyao Jiang, AA Clerk, and JGE Harris, “Non-reciprocal control and cooling of phonon modes in an optomechanical system,” *Nature* **568**, 65–69 (2019).
- [20] Diego Porras and Samuel Fernández-Lorenzo, “Topological amplification in photonic lattices,” *Phys. Rev. Lett.* **122**, 143901 (2019).
- [21] Freek Ruesink, Mohammad-Ali Miri, Andrea Alu, and Ewold Verhagen, “Nonreciprocity and magnetic-free isolation based on optomechanical interactions,” *Nature communications* **7**, 1–8 (2016).
- [22] Shabir Barzanjeh, Matteo Aquilina, and André Xuereb, “Manipulating the flow of thermal noise in quantum devices,” *Phys. Rev. Lett.* **120**, 060601 (2018).
- [23] A. McDonald, T. Pereg-Barnea, and A. A. Clerk, “Phase-dependent chiral transport and effective non-hermitian dynamics in a bosonic kitaev-majorana chain,” *Phys. Rev. X* **8**, 041031 (2018).
- [24] Clara C. Wanjura, Matteo Brunelli, and Andreas Nunnenkamp, “Topological framework for directional amplification in driven-dissipative cavity arrays,” *arXiv e-prints*, arXiv:1909.11647 (2019), arXiv:1909.11647 [cond-mat.mes-hall].
- [25] Yi-Pu Wang, J. W. Rao, Y. Yang, Peng-Chao Xu, Y. S. Gui, B. M. Yao, J. Q. You, and C.-M. Hu, “Nonreciprocity and unidirectional invisibility in cavity magnonics,” *Phys. Rev. Lett.* **123**, 127202 (2019).
- [26] Daniel Malz, László D. Tóth, Nathan R. Bernier, Alexey K. Feofanov, Tobias J. Kippenberg, and Andreas Nunnenkamp, “Quantum-limited directional amplifiers with optomechanics,” *Phys. Rev. Lett.* **120**, 023601 (2018).
- [27] Shunyu Yao and Zhong Wang, “Edge states and topological invariants of non-hermitian systems,” *Phys. Rev. Lett.* **121**, 086803 (2018).
- [28] Kazuki Yokomizo and Shuichi Murakami, “Non-bloch band theory of non-hermitian systems,” *Phys. Rev. Lett.* **123**, 066404 (2019).
- [29] Ching Hua Lee and Ronny Thomale, “Anatomy of skin modes and topology in non-hermitian systems,” *Phys. Rev. B* **99**, 201103 (2019).
- [30] Shunyu Yao, Fei Song, and Zhong Wang, “Non-hermitian chern bands,” *Phys. Rev. Lett.* **121**, 136802 (2018).
- [31] Stefano Longhi, “Probing non-hermitian skin effect and non-bloch phase transitions,” *Phys. Rev. Research* **1**, 023013 (2019).
- [32] Zhesen Yang, Kai Zhang, Chen Fang, and Jiangping Hu, “Auxiliary generalized Brillouin zone method in non-Hermitian band theory,” *arXiv e-prints*, arXiv:1912.05499 (2019), arXiv:1912.05499 [cond-mat.mes-hall].
- [33] S. Longhi, “Non-bloch-band collapse and chiral zener tunneling,” *Phys. Rev. Lett.* **124**, 066602 (2020).
- [34] Kohei Kawabata, Nobuyuki Okuma, and Masatoshi Sato, “Non-Bloch band theory of non-Hermitian Hamiltonians in the symplectic class,” *arXiv e-prints*, arXiv:2003.07597 (2020), arXiv:2003.07597 [cond-mat.mes-hall].
- [35] Tian-Shu Deng and Wei Yi, “Non-bloch topological invariants in a non-hermitian domain wall system,” *Phys. Rev. B* **100**, 035102 (2019).
- [36] Ching Hua Lee, Linhu Li, Ronny Thomale, and Jiangbin Gong, “Unraveling non-Hermitian pumping: emergent spectral singularities and anomalous responses,” *arXiv e-prints*, arXiv:1912.06974 (2019), arXiv:1912.06974 [cond-mat.mes-hall].
- [37] Fei Song, Shunyu Yao, and Zhong Wang, “Non-hermitian topological invariants in real space,” *Phys. Rev. Lett.* **123**, 246801 (2019).
- [38] Markus Aspelmeyer, Tobias J. Kippenberg, and Florian Marquardt, “Cavity optomechanics,” *Rev. Mod. Phys.* **86**, 1391–1452 (2014).
- [39] Mattias Fitzpatrick, Neereja M Sundaresan, Andy CY Li, Jens Koch, and Andrew A Houck, “Observation of a dissipative phase transition in a one-dimensional circuit qcd lattice,” *Physical Review X* **7**, 011016 (2017).
- [40] See the Supplemental Material.
- [41] Heinrich-Gregor Zirnstein, Gil Refael, and Bernd Rosenow, “Bulk-boundary correspondence for non-Hermitian Hamiltonians via Green functions,” *arXiv e-prints*, arXiv:1901.11241 (2019), arXiv:1901.11241 [cond-mat.mes-hall].
- [42] Flore K. Kunst, Elisabet Edvardsson, Jan Carl Budich, and Emil J. Bergholtz, “Biorthogonal bulk-boundary correspondence in non-hermitian systems,” *Phys. Rev. Lett.* **121**, 026808 (2018).
- [43] Tobias Helbig, Tobias Hofmann, Stefan Imhof, Mohamed Abdelghany, Tobias Kiessling, Laurens W. Molenkamp, Ching Hua Lee, Alexander Szameit, Martin Greiter, and Ronny Thomale, “Observation of bulk boundary correspondence breakdown in topoelectrical circuits,” *arXiv e-prints*, arXiv:1907.11562 (2019), arXiv:1907.11562 [cond-mat.mes-hall].
- [44] Lei Xiao, Tianshu Deng, Kunkun Wang, Gaoyan Zhu, Zhong Wang, Wei Yi, and Peng Xue, “Non-Hermitian bulk-boundary correspondence in quantum dynamics,” *Nat. Phys.* (2020), arXiv e-prints, arXiv:1907.12566 (2019).
- [45] Ananya Ghatak, Martin Brandenbourger, Jasper van Wezel, and Corentin Coulais, “Observation of non-Hermitian topology and its bulk-edge correspon-

- dence,” arXiv e-prints , arXiv:1907.11619 (2019), arXiv:1907.11619 [cond-mat.mes-hall].
- [46] Kai Zhang, Zhesen Yang, and Chen Fang, “Correspondence between winding numbers and skin modes in non-hermitian systems,” arXiv e-prints , arXiv:1910.01131 (2019), arXiv:1910.01131 [cond-mat.mes-hall].
- [47] Nobuyuki Okuma, Kohei Kawabata, Ken Shiozaki, and Masatoshi Sato, “Topological origin of non-hermitian skin effects,” *Phys. Rev. Lett.* **124**, 086801 (2020).

Supplemental Material

DERIVATION OF THE EFFECTIVE NON-HERMITIAN HAMILTONIAN

By the definition of ϕ_i , we have

$$\dot{\phi}_i = \frac{d}{dt} \text{Tr}[a_i \rho(t)] = \text{Tr}[a_i \dot{\rho}(t)]. \quad (16)$$

Inserting the master equation

$$\dot{\rho}(t) = -i[H_0, \rho] + \sum_{\mu} \left(L_{\mu} \rho L_{\mu}^{\dagger} - \frac{1}{2} \{L_{\mu}^{\dagger} L_{\mu}, \rho\} \right), \quad (17)$$

we obtain

$$\begin{aligned} \dot{\phi}_i &= -i \text{Tr}([a_i, H_0] \rho(t)) \\ &+ \frac{1}{2} \sum_{\mu} \text{Tr}([L_{\mu}^{\dagger}, a_i] L_{\mu} \rho(t) + L_{\mu}^{\dagger} [a_i, L_{\mu}] \rho(t)). \end{aligned} \quad (18)$$

Now we take the Hamiltonian

$$H_0 = \sum_{i,j} (h_0)_{ij} a_i^{\dagger} a_j + \sum_i (\epsilon_i a_i^{\dagger} + \epsilon_i^* a_i), \quad (19)$$

and the dissipators

$$\{L_{\mu}\} = \{L_i^l, L_i^g\}, \quad (20)$$

with

$$L_i^l = \sum_j D_{ij}^l a_j; \quad L_i^g = \sum_j D_{ij}^g a_j^{\dagger}. \quad (21)$$

The specific system shown in Fig. 1(a) of the main article is a special case of this general model. The first term in Eq. (18) is

$$-i \text{Tr}([a_i, H_0] \rho(t)) = -i \sum_j (h_0)_{ij} \phi_j - i \epsilon_i. \quad (22)$$

For the second term in Eq. (18), only the loss dissipators L_i^l contribute:

$$\begin{aligned} \sum_m [L_m^{\dagger}, a_i] L_m^l &= \sum_{m,n} D_{mn}^{l*} [a_n^{\dagger}, a_i] L_m^l \\ &= - \sum_m D_{mi}^{l*} L_m^l \\ &= - \sum_{m,j} D_{mi}^{l*} D_{mj}^l a_j, \end{aligned} \quad (23)$$

while for the third term, only the gain dissipators L_i^g contribute:

$$\begin{aligned} \sum_m L_m^g [a_i, L_m^g] &= \sum_{m,n} L_m^g [a_i, D_{mn}^g a_n^{\dagger}] \\ &= \sum_m D_{mi}^g L_m^g \\ &= \sum_{m,j} D_{mi}^g D_{mj}^{g*} a_j, \end{aligned} \quad (24)$$

therefore, the second and third terms of Eq. (18) are simplified to

$$\frac{i}{2} ((D^{g\dagger} D^g)^T - D^{l\dagger} D^l)_{ij} \phi_j. \quad (25)$$

Summing up these terms, Eq. (18) becomes

$$\dot{\phi}_i = -i \sum_j H_{ij} \phi_j - i \epsilon_i, \quad (26)$$

with the effective non-Hermitian Hamiltonian

$$H = h_0 + \frac{i}{2} ((D^{g\dagger} D^g)^T - D^{l\dagger} D^l). \quad (27)$$

For our specific model, the nonzero parameters are $(h_0)_{i,i+1} = (h_0)_{i+1,i} = t_1$, $(h_0)_{i,i+2} = (h_0)_{i+2,i} = t_2$, $(h_0)_{ii} = \omega_0$, $D_{i,i}^l = \sqrt{\gamma}$, $D_{i,i+2}^l = -i\sqrt{\gamma}$ and $D_{i,i}^g = \sqrt{\gamma'}$. It follows from Eq. (27) that the effective non-Hermitian Hamiltonian H is Eq. (4). We note that under the open-boundary condition (OBC), while diagonal elements in the bulk are all $\omega_0 + i\kappa = \omega_0 + i(\gamma'/2 - \gamma)$, the four edge-site diagonal elements $H_{00}, H_{11}, H_{L-1,L-1}, H_{LL} = \omega_0 + i(\gamma' - \gamma)/2$. For simplicity, we let these four elements be $\omega_0 + i\kappa$, which does not cause any appreciable modification of our main results (While this is intuitively apparent, we have also numerically confirmed it). The H operator reads

$$H = \begin{pmatrix} \omega_0 + i\kappa & t_1 & t_2 - \frac{\gamma}{2} & 0 & \cdots \\ t_1 & \omega_0 + i\kappa & t_1 & t_2 - \frac{\gamma}{2} & \cdots \\ t_2 + \frac{\gamma}{2} & t_1 & \omega_0 + i\kappa & t_1 & \cdots \\ 0 & t_2 + \frac{\gamma}{2} & t_1 & \omega_0 + i\kappa & \cdots \\ \cdots & \cdots & \cdots & \cdots & \cdots \end{pmatrix} \quad (28)$$

To simplify the expressions, we measure the frequency with respect to ω_0 , i.e., shift the frequency (energy) $\omega \rightarrow \omega - \omega_0$:

$$H = \begin{pmatrix} i\kappa & t_1 & t_2 - \frac{\gamma}{2} & 0 & \cdots \\ t_1 & i\kappa & t_1 & t_2 - \frac{\gamma}{2} & \cdots \\ t_2 + \frac{\gamma}{2} & t_1 & i\kappa & t_1 & \cdots \\ 0 & t_2 + \frac{\gamma}{2} & t_1 & i\kappa & \cdots \\ \cdots & \cdots & \cdots & \cdots & \cdots \end{pmatrix}. \quad (29)$$

We could also include more dissipators such as $\sqrt{\gamma_1}(a_j - ia_{j+2})$, $\sqrt{\gamma_2}(a_j + ia_{j+2})$, $\sqrt{\gamma_3}(a_j^{\dagger} + ia_{j+2}^{\dagger})$, $\sqrt{\gamma_4}(a_j^{\dagger} - ia_{j+2}^{\dagger})$, $\sqrt{\gamma_1'} a_j^{\dagger}$, $\sqrt{\gamma_2'} a_j$, and it is straightforward to obtain a similar H , except that the diagonal elements become $H_{ii} = (\gamma_1' - \gamma_2')/2 - \gamma_1 - \gamma_2 + \gamma_3 + \gamma_4$, and $H_{i,i\pm 2}$ become $t_2 \pm (\gamma_2 + \gamma_3 - \gamma_1 - \gamma_4)/2$. Our Fig. 1 in the main article corresponds to the special case $\gamma_1 = \gamma$, $\gamma_1' = \gamma'$ with other γ 's vanishing.

DERIVATION OF THE GBZ FORMULA

We now derive Eq.(11). For a given Laurent polynomial $f(\beta) = \sum_j f_j \beta^j$, one can define a matrix

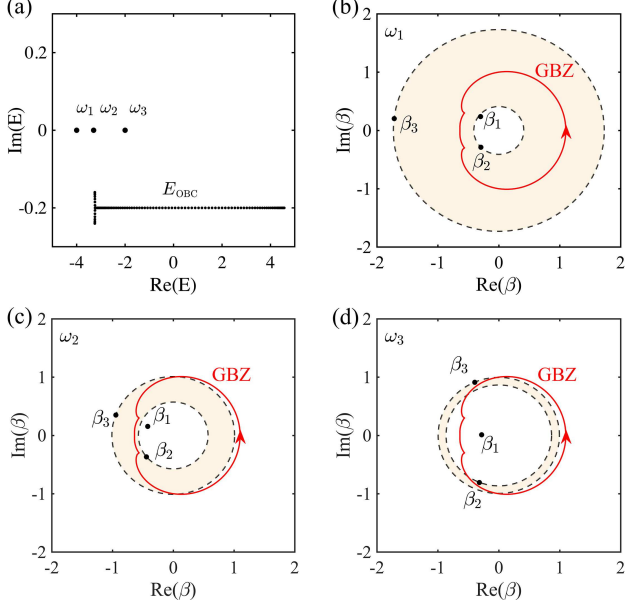


FIG. 3. GBZ and roots of $h(\beta) = \omega$. (a) The OBC energy spectra E_{OBC} , and frequencies $\omega_{1,2,3}$ used in (b,c,d). Values of t_1, t_2, γ are the same as in Fig.2, and $\kappa = -0.2$ (Stability requires that the imaginary parts of energies are negative, which is satisfied when $\kappa < -0.04$). (b,c,d) The roots $\beta_{1,2,3}$ for $\omega_1 = -4, \omega_2 = -3.3$, and $\omega_3 = -2$. The fourth root β_4 is not shown for being outside this region.

$T(f)$ (known as a Toeplitz matrix) whose elements are $T_{jk}(f) = f_{k-j}$, or $T_{jk}(f) = \int_{|\beta|=R} \frac{d\beta}{2\pi i \beta} \beta^{j-k} f(\beta)$ for an arbitrary radius R . The rank of T is the chain length in our work, i.e. $j, k = 0, \dots, L$. We have $\omega - H = T(\omega - h(\beta))$ by definition, and our task is to calculate its inverse, G . To this end, we use a product identity $T(f)T(g) = T(fg)$ for two Laurent polynomials f and g . This can be proved by $\sum_k T_{ik}(f)T_{kj}(g) = \sum_k f_{k-i}g_{j-k} = (fg)_{j-i} = T_{ij}(fg)$ (There are some corrections near the boundaries $i, j = 0$ or L , which will not be our focus). As a corollary, we have $T(f)T(f^{-1}) = T(1)$ and $[T(f)]^{-1} = T(f^{-1})$. We may formally take $f = \omega - h(\beta)$, then $G = T(\frac{1}{\omega - h(\beta)})$, and consequently

$$G_{xy} = \int_{|\beta|=R} \frac{d\beta}{2\pi i \beta} \frac{\beta^{x-y}}{\omega - h(\beta)}. \quad (30)$$

This means expanding $\frac{1}{\omega - h(\beta)}$ as a Laurent series and the coefficients are G_{xy} . However, as a mathematical fact, the Laurent series depends on R . In fact, in $T(f)T(f^{-1}) = T(1)$, the proper Laurent series for f^{-1} should be obtained as follows. We find a smooth interpolation $f_t(\beta)$ between $f_1(\beta) = f(\beta)$ and the trivial polynomial $f_0(\beta) = 1$, for which we know that $T(f_0)T(f_0^{-1}) = T(1)$ is trivially true. The proper Laurent series for $f_1^{-1}(\beta) = f^{-1}(\beta)$ is then obtained from the interpolation $f_t^{-1}(\beta)$. The smoothness of interpolation means that $f_t(\beta) \neq 0$ on the circle $|\beta| = R$. The

existence of such an interpolation requires that the phase winding number $\frac{1}{2\pi} \int_{|\beta|=R} d \arg[f(\beta)] = 0$ because, as a topological invariant, it stays constant and f_0 apparently has vanishing winding number. Let us factorize

$$\omega - h(\beta) = \frac{c \prod_{j=1}^{2M} (\beta - \beta_j)}{\beta^M}, \quad (31)$$

where $\beta_{j=1, \dots, 2M}$ stand for the roots of $\omega - h(\beta) = 0$ and c is a constant. It follows that the vanishing of winding number requires taking R within $|\beta_M| < R < |\beta_{M+1}|$ [colored region in Fig.3(b,c,d)]. Thus the circle $|\beta| = R$ encloses β_1, \dots, β_M . As discussed before, the GBZ encloses the same roots, therefore, we can replace the integration contour in Eq.(30) by the GBZ, resulting in Eq.(11). Notably, although the eligible R region in Eq.(30) varies with ω [see Fig.3(b,c,d)], Eq.(11) remains valid with the same GBZ for all ω .

AMPLIFICATION WITH FREQUENCY-INDEPENDENT DIRECTIONALITY

In the main article, we focused on the case that the amplification direction depends on the frequency. As mentioned there, the same model also supports directional amplification with frequency-independent directionality. In fact, this can be achieved by taking different parameter values in the same model; an example is given in Fig.4. For this choice of parameter values, the GBZ has no intersection with BZ, therefore, the amplification has to be unidirectional within the entire bandwidth.

EFFECT OF ZERO MODES

In the main article, we considered a single-band model without topological edge mode, for which the directional amplification comes solely from the continuous band. Here, for completeness, we consider a model with topological edge modes. We show that the zero modes have a visible contribution within a small frequency window when the chain is short, and its effect diminishes as the chain becomes longer. As such, the effect of zero mode is negligible in a long chain.

Specifically, we consider a two-band model introduced in Ref.[37], with the Bloch Hamiltonian:

$$\begin{aligned} H(k) &= d_x(k)\sigma_x + d_y(k)\sigma_y + i\kappa; \\ d_x(k) &= t_1 + (t_2 + t_3) \cos k + i\frac{\gamma}{2} \sin k \\ d_y(k) &= (t_1 - t_3) \sin k + i\frac{\gamma}{2} \cos k. \end{aligned} \quad (32)$$

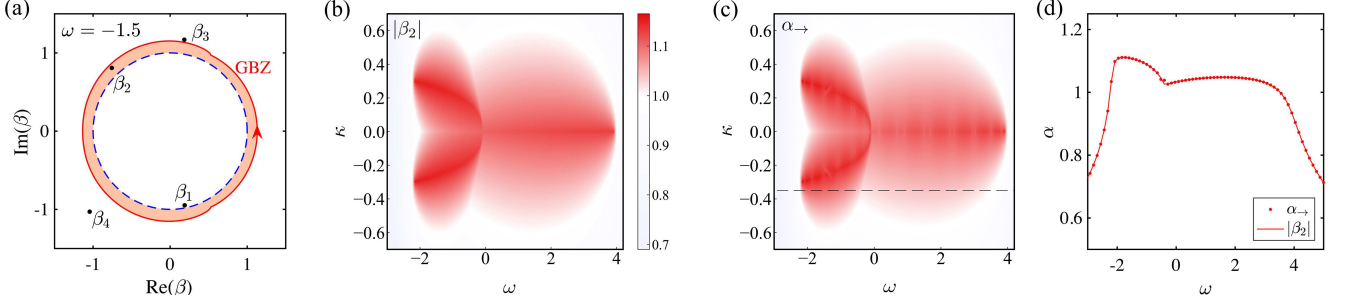


FIG. 4. Directional amplification with a frequency-independent directionality. Parameter values are $t_1 = 1, t_2 = 1, \gamma = 0.6$. (a) GBZ. The locations of roots of $\omega - h(\beta) = 0$ are shown for $\kappa = -0.35$ and $\omega = -1.5$. (b) $|\beta_2|$ as a function of κ and ω . (c) α_+ as a function of κ and ω , which is in agreement with the theory of (b). (d) Detailed comparison of α_+ and $|\beta_2|$ along the cut $\kappa = -0.35$ [dashed line in (c)].

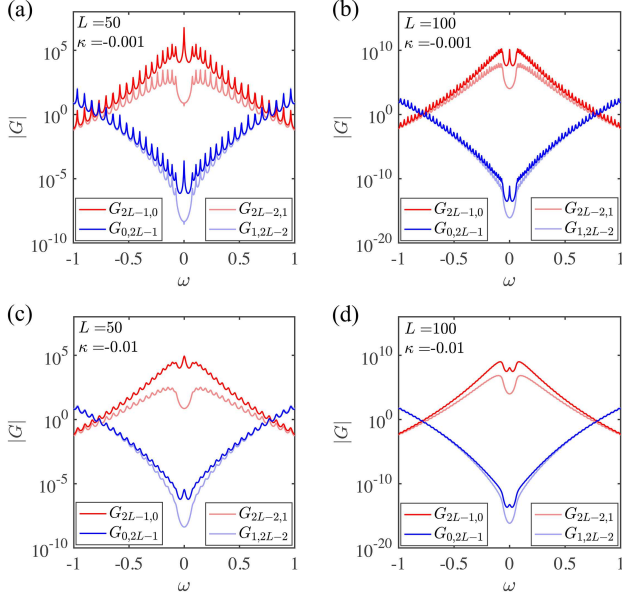


FIG. 5. G_{xy} for $x, y = 0, 1, 2L-2, 2L-1$. Parameter values are $t_1 = 1.2, t_2 = 1, t_3 = 0.2, \gamma = 0.3$. (a) $\kappa = -0.001, L = 50$. (b) $\kappa = -0.001, L = 100$. (c) $\kappa = -0.01, L = 50$. (d) $\kappa = -0.01, L = 100$.

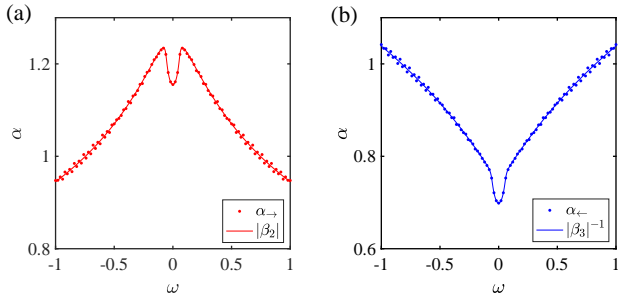


FIG. 6. Comparison of our formula and brute-force numerical results for the two-band model. (a) α_+ and $|\beta_2|$. (b) α_- and $|\beta_3|^{-1}$. Parameter values are $t_1 = 1.2, t_2 = 1, t_3 = 0.2, \gamma = 0.3, \kappa = -0.01$.

The real-space OBC Hamiltonian is

$$H = \begin{pmatrix} h_0 & h_1 & 0 & 0 & \cdots \\ h_{-1} & h_0 & h_1 & 0 & \cdots \\ 0 & h_{-1} & h_0 & h_1 & \cdots \\ 0 & 0 & h_{-1} & h_0 & \cdots \\ \cdots & \cdots & \cdots & \cdots & \cdots \end{pmatrix} \quad (33)$$

in which

$$\begin{aligned} h_0 &= t_1 \sigma_x + i\kappa \\ h_1 &= \frac{t_2 + t_3 + \gamma/2}{2} \sigma_x + i \frac{\gamma/2 - t_2 + t_3}{2} \sigma_y \\ h_{-1} &= \frac{t_2 + t_3 - \gamma/2}{2} \sigma_x + i \frac{\gamma/2 + t_2 - t_3}{2} \sigma_y. \end{aligned} \quad (34)$$

We consider an OBC chain with L unit cells, with each unit cell containing two sites $2j, 2j+1$ ($j = 0, 1, \dots, L-1$). The even and odd sites correspond to $\sigma_z = 1$ and -1 , respectively. To see the effects of zero modes, we calculate G_{xy} for $x, y = 0, 1, 2L-2, 2L-1$ (Fig. 5). A peak is found at $\omega = 0$ for $G_{0,2L-1}$ and $G_{2L-1,0}$. This peak is not seen in $G_{1,2L-2}$ and $G_{2L-2,1}$, which is an evidence that it stems from the topological zero modes. In fact, each topological zero mode has a chirality, meaning that it is an eigenstate of σ_z . Specifically, the zero modes in our model, as eigenstates of σ_z , have vanishing weight at $x = 1$ and $x = 2L-2$. As such, $G_{1,2L-2}$ and $G_{2L-2,1}$ are insensitive to the zero modes, which explains the absence of zero-mode peak. A more significant feature is the length dependence of zero-mode peak. Comparing Fig.5 (a) and (b), or (c) and (d), we see that the zero-mode peak diminishes as the chain length grows. This is intuitive because the effects of topological zero modes are expected to be significant only near the edges.

To compare the numerical results and our theory, we plot α_+, α_- in Fig.6, which are in excellent agreement with our formulas. Note that $h(\beta)$ is a matrix and $\beta_{j=1,2,3,4}$ are the roots of $\det[\omega - h(\beta)] = 0$.